Original Paper

Stability of Gaomiaozi bentonite: Interlayer hydration structure and aggregation morphology

Zhaomin Tan[1], Chengyun Fu[1], Mark Julian Henderson[2], Xuezhi Dai[1] ◍, Jianfeng Cheng[3,4], Jingli Xie[3,4], Shan Zhu[1] and Minhao Yan[2] ◍

[1]School of Materials and Chemistry, Southwest University of Science and Technology, Mianyang, China; [2]State Key Laboratory of Environment-Friendly Energy Materials, Southwest University of Science and Technology, Mianyang, China; [3]Beijing Research Institute of Uranium Geology, Beijing, China and [4]CAEA Innovation Center for Geological Disposal of High-Level Radioactive Waste, Beijing, China

Abstract

The sustainability of high-level radioactive waste repositories situated in fractured crystalline rocks depends on the stability of bentonite liners, and this can pose a problem in certain groundwater conditions that favor the formation of colloids from backfill materials that are prone to erosion. The influence of different environments on the structure of Gaomiaozi bentonite (GMZ) and GMZ colloids (GMZC) is presented here. Different hydrated interlayer structures of bulk and colloidal forms of this bentonite from small-angle X-ray scattering (SAXS) data are demonstrated. Analysis of the scattering data showed that GMZ had three interlayer water structures: dehydrated (0W), monohydrated (1W), and bi-hydrated (2W). The colloids readily agglomerated at acidic pH (pH <5) but showed resistance to agglomeration in an alkaline condition (pH >7). The effect of Na^+, K^+, Mg^{2+}, and Ca^{2+} on the lamellar structure and agglomerate morphology of GMZC particles was investigated. In general, the tendency of colloids to agglomerate was greater in the presence of divalent metal cations compared with monovalent metal cations. High concentrations (10^{-5} to 10^{-3} mol L^{-1}) of divalent ions imparted order into the stacked lamellar structure after the saturation of the interlayer. In contrast, monovalent ions reduced the tendency of the particles to aggregate, leading to an abundance of colloidal nanoparticles prone to erosion. This work helps to better understand the structural characteristics of GMZC in the groundwater environment, and provides a valuable reference for the evaluation of nuclide migration in the deep geological disposal of high-level radioactive wastes.

Keywords: bentonite colloids; cations; interlayer water; small-angle X-ray scattering

(Received: 20 January 2024; revised: 29 February 2024; accepted: 22 March 2024)

Introduction

The safe disposal of high-level radioactive waste (HLW) is a challenge facing the development of nuclear energy (Long and Ewing, 2004; Darda *et al.*, 2021). Deep geological disposal is the internationally recognized and feasible method for HLW at present. Deep geological repositories for HLW are typically located several hundred to several thousand meters underground and are reinforced with multiple barriers to achieve long-term or permanent isolation of the waste from the environment (SKB, 2010; Wang, 2010; Serie, 2022). The host rock that surrounds a repository can form a natural barrier, and, together with the engineered barriers composed of buffer/backfill materials, the high-level waste storage container, and solidified state of the waste, this natural rock barrier helps to ensure the retention of radioactive waste. The buffer/backfill materials keep the waste tanks from coming into direct contact with the surrounding environment. For the construction of engineered barriers, in many countries, bentonite is selected as the preferred buffer/backfill material (Bucher and Müller-Vonmoos, 1989; Villar and Lloret, 2008; Missana *et al.*, 2011).

In addition to fractures naturally present in the host rock, fractures can be induced during repository construction. These fractures present possible channels through which groundwater can seep into the rock, causing clay colloids to form by erosion of bentonite by groundwater. Clay colloids form by erosion of bentonite by groundwater (Degueldre *et al.*, 1996; Missana *et al.*, 2003; Baik *et al.*, 2007; Albarran *et al.*, 2014). These colloids reduce the density of the bentonite in the tunnels of a disposal repository, threatening the long-term safety of the repository. The formation rate of bentonite colloids largely depends on groundwater qualities such as the acidity (Kretzschmar *et al.*, 1998; Tombácz and Szekeres, 2004), salinity (Swartzen-Allen and Matijevic, 1976; Huynh and Chen, 2011; Huangfu *et al.*, 2013), and colloid type (Missana *et al.*, 2018a). Zhu *et al.* (2022) show that colloid formation is strongly inhibited in high-salinity and complex ionic environments rich in Na^+. Xu *et al.* (2018) confirm the

reversibility of the effects of pH and electrolytes on colloid formation, suggesting the dynamic effect of water on the colloids as the water chemistry changes. These external factors also affect the adsorption capacity of the colloids for radionuclides as the colloids migrate (Bouby *et al.*, 2011; Zuo *et al.*, 2017; Yin *et al.*, 2018). Therefore, investigating the behavior of colloids in different aqueous environments and the effect of these environmental factors on the stability of colloids will help to gain a deeper understanding of the migration behavior of colloids and to evaluate the safety of disposal repositories.

Gaomiaozi (GMZ) bentonite is the buffer/backfill material proposed for the Beishan Geological Disposal Repository in China. GMZ bentonite is composed of montmorillonite (75.4%), and the secondary minerals quartz (11.7%), cristobalite (7.3%), feldspar (4.3%), kaolinite (0.8%), and calcite (0.5%) (S. Zhu *et al.*, 2022). The montmorillonite has a particle diameter of 100–350 nm with a surface electric potential (ζ) of −30 to −50 mV (Plaschke *et al.*, 2001; Missana *et al.*, 2018b; Xian *et al.*, 2020; Wang *et al.*, 2022). Studies on the stability of GMZ bentonite (Xian *et al.*, 2020; Xu *et al.*, 2018) have investigated the effects of the pH, ionic strength, and ion type on the aggregation kinetics of GMZ colloids. In addition, Pinnavaia *et al.* (1984) performed small-angle neutron scattering analysis on the layered structure and pore size of pillared clay and concluded that the stack thickness of these layered colloidal particles can be calculated using appropriate models. Ferrage *et al.* (2018) analyzed the small-angle neutron scattering spectra of the dehydrated structure (0W), monohydrated (1W), and bi-hydrated (2W) of vermiculite. They discovered that changes in the hydration structure led to a shift in the characteristic peaks in the high q region (q is a function of the scattering vector magnitude for the small-angle scattering), while changes in the power law index in the mid-q region indicate an anisotropic arrangement of the particles and particle defects. While these results help to understand the colloidal behavior of GMZ bentonite colloids, few studies have been performed on the *in situ* layered structure of water-borne bentonite colloids. Bentonite is a typical material with a layered structure. Given that bentonites in backfill will be in contact with water, it is important to understand the changes in its *in situ* layered structure in water as a result of environmental factors.

To better predict the migration behavior of nuclides on colloids in the repository environment, it is necessary to understand the swelling/collapsing behavior of GMZC which can generate additional preferential pathways for nuclides transfer (Bradford *et al.*, 2003; Ferrage, 2016). The structural properties of bentonite colloids in aqueous solutions were studied as a function of pH, cation concentration and charge. The stability and structure of GMZC were analyzed with emphasis. Small-angle X-ray scattering (SAXS) was used to reveal the structural changes of GMZC in different valence environments. The environmental behavior of GMZC is explained and used as a reference for safety assessment of HLW.

Materials and methods

Colloid preparation

The GMZ bentonite used in this study was obtained from Xinghe County, Inner Mongolia, China, and was supplied by the China Institute for Radiation Protection. The bulk bentonite sample was crushed into powder using an agate mortar and was passed through a 400-mesh sieve. The bentonite colloids were prepared by gravity as follows. GMZ bentonite powder (5 g) was dissolved in 500 mL of deionized water (resistivity ≥18.4 MΩ·cm). The mixture was sonicated in a water bath for 2 h to ensure the thorough dispersion of the bentonite powder. The mixture was sealed and stored in a glass vessel for 3 days. The supernatant was separated and allowed to stand. The lower layer of residues was discarded. This process was repeated once every 3 days until no more large precipitates appeared in the bottom colloidal phase after more than 15 days (S. Zhu *et al.*, 2022).

The colloids were further purified to eliminate the possible interference from dissolved salt ions introduced by colloids in the subsequent experimental steps. Colloids under 250 nm in size were extracted and used in the experiment. The colloids were dialyzed against deionized water for 3 days. After dialysis, the GMZC with a conductivity of below 20 μS cm^{-1} were stored in a glass vessel. Other reagents used for colloid preparation were analytical grade and did not require further purification.

Aggregate morphology

All the chemicals used in experiments were A.R. grade, supplied from Chengdu KeLong Chemical Co. Ltd., China without any further purification. Stock solutions of NaCl, KCl, MgCl$_2$, and CaCl$_2$ (0.5 mol L^{-1}) prepared using 18.4 MΩ·cm quality water were used to prepare the diluted solutions. Different proportions of stock solution were added to GMZ colloidal dispersions with various cationic concentrations, from 10^{-5} to 10^{-3} mol L^{-1}. The prepared colloidal solutions were mixed in a shaker for 2 h and were left to stand for 3 days before the measurement was conducted. The pH of the colloids was adjusted (to pH 2 and pH 12) by adding different volumes of 0.1 and 0.5 mol L^{-1} NaOH and HNO$_3$, and the pH and conductivity of the GMZ colloids were measured using a Thermo Fisher XL200 meter.

Colloid characterization

The morphology of the GMZ bentonite powder was revealed using a field-emission transmission electron microscope (Libra 200FE, Zeiss, Germany; magnification range: 80–10^6; operating voltage: 200 kV). The mineralogical characteristics of the colloid samples (dried at 60°C, oriented powders deposited on glass slides) were obtained by X-ray diffraction (XRD) (Ultima IV, Rigaku, Japan; Cu-Kα, λ = 0.154 nm). The colloidal particle size and zeta potential were measured using a multi-angle particle size and zeta potential analyzer (Omni, Brookhaven, USA; light source wavelength: λ = 640 nm). The hydrodynamic radius, R_H, of the bentonite colloids was calculated using the Stokes-Einstein equation:

$$R_H = \frac{k_B T}{6\pi\eta D_t}, \tag{1}$$

where k$_B$ is the Boltzmann constant (1.38064852×10^{-23} J K^{-1}), T is the temperature, η is the viscosity of the solution, and D_t is the diffusion coefficient.

An Anton-Paar SAXSpace (Austria, 40 kV, 50 mA, Cu-Kα, λ = 0.1542 nm) instrument was used to quantify the nanoscale colloidal structure. The scattered rays were collected on a Myshen2 detector (Detris, Switzerland). The colloidal samples were placed in a quartz capillary (1 mm inner diameter) and were measured for over 30 min to obtain the SAXS data. The raw data were normalized using SAXSquant (version 4.1.0.7505). The background scattering from the capillary and deionized water was removed.

The scattering intensity $I(q)$ was measured as a function of the scattering vector magnitude (Guinier *et al.*, 1979):

$$q = \frac{4\pi \sin\theta}{\lambda}. \tag{2}$$

I and the interlayer space (d) were obtained from:

$$d = \frac{2\pi}{q}. \tag{3}$$

For randomly oriented thin plates or discs, for example clay colloids, the Guinier approximation at low Q values for the scattering intensity distribution is:

$$I = I_e V^2 \rho_0^2 \frac{8}{q^2 R^2} \exp\left[-\frac{q^2(2H)^2}{12}\right], \tag{4}$$

where I_e is the intensity scattered by one electron, V is particle volume, ρ_0 is mean particle density, and H is the thickness of the disc.

Results and Discussion

Characterization of GMZ bentonite colloids

The properties of the GMZC used in this study are presented in Table 1. The mass fraction showed the concentration of GMZ bentonite in water. It was determined in triplicate by evaporating the water from 80 mL aliquots of GMZC dispersions in an oven at 80°C for at least 4 days.

The morphology and size of GMZ bentonite particles were determined by transmission electron microscopy (TEM); see Fig. 1a. A zoom-in of one edge (Fig. 1b) has some indentations and evidence of stacked layers at the upturned edge of the crystal. Dehydration of the sample during preparation for microscopy precluded an accurate determination of the layer number and interlayer space. Consequently, SAXS was used to characterize the layered structures of the GMZ and GMZC.

Table 1. Summary of data for the GMZ colloid parameters

pH	Hydrodynamic particle diameter (nm)	Conductivity (μS cm^{-1})	Zeta potential (mV)	Mass fraction (%)
6.7	211±5	5.6±0.1	−45.2±2.1	0.5

Change in hydration of GMZ bentonite

The effect of temperature on SAXS from GMZ bentonite at 25 and 300°C are shown in Fig. 2. Two characteristic peaks are present in the pattern of the GMZ at room temperature (25°C). The broad peak at ~4 nm^{-1} indicates overlapped peaks due to the scattering interference among the particles. This feature suggests the presence of non-uniform particle size or spacing. Further fitting of the broad peak yielded two smaller peaks.

The d-spacings corresponding to peaks at 0.92, 1.27, and 1.45 nm (Fig. 2) are attributed to different interlayer hydration structures. The Na$^+$ ions between the bentonite layers serve to balance the electric potential and exhibit strong water absorption. They combine with water molecules to form different hydration structures, giving rise to variations in the interlayer spacing. To confirm the origin of these two peaks in the GMZ spectrum at room temperature (25°C), GMZ powder was heated at 300°C (Hong *et al.*, 2020). Compared with 25°C, the interlayer spacing of the GMZ is smaller at 300°C (Fig. 2). The high temperature evaporated the interlayer water (Ferrage *et al.*, 2007), and the interlayer of the GMZC was dehydrated and changed from a multi-hydration structure to a waterless interlayer structure. Based on this result, it is inferred that at 25°C, the three peaks in the GMZ powder spectrum correspond to three different interlayer hydration structures (Morida *et al.*, 2023), i.e. the

Figure 2. SAXS curves obtained from GMZ powders in 300°C (red open circles) and 25°C (black filled circles). The peak indicated that GMZ particles have a lamellar structure.

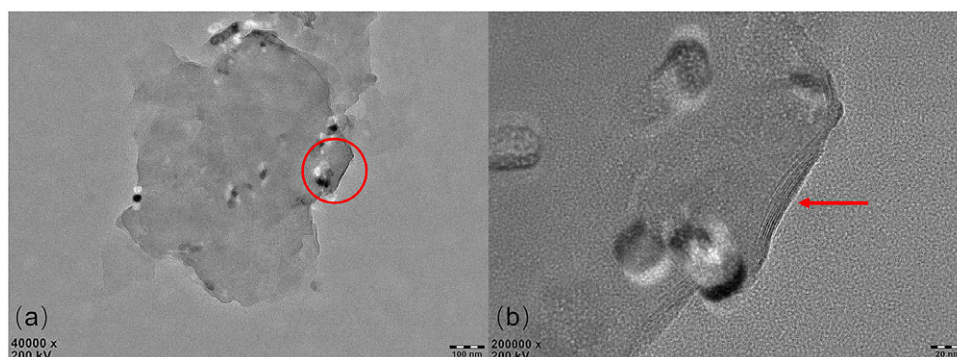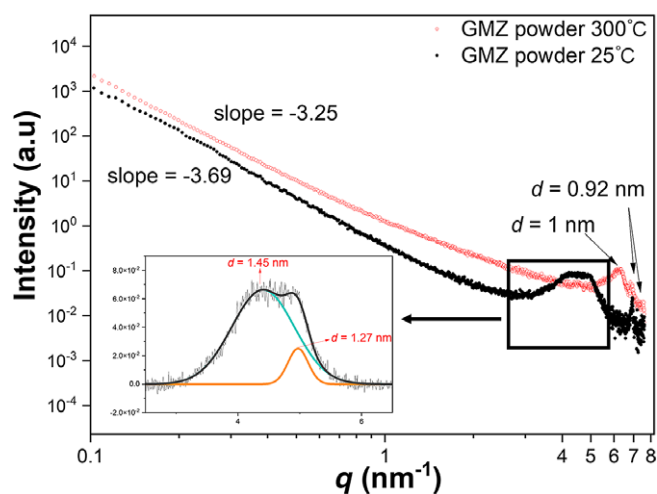**Figure 1.** TEM images of GMZ bentonite: the particle (a) and details (b); the arrow shows the layered structure.

dehydrated (0W, *d*-space = 0.92 nm), monohydrated (1W, *d*-space = 1.27 nm), and bi-hydrated (2W, *d*-space = 1.46 nm). The GMZ powder spectrum contains two characteristic peaks at 300°C, corresponding to interlayer spacing values of 1.00 and 0.92 nm. The peak with *d*-spacing of 1.00 nm might correspond to the 0W structure formed via dehydration of the 2W structure, while the *d*-spacing of 0.92 nm corresponds to the spacing of the original GMZ powder without interlayer water or Na$^+$ (Meunier, 2006; Brochard, 2021). The 001 peak of sodium bentonite typically indicates an interlayer spacing of 1.25 nm (Zhang *et al.*, 2014; Verma *et al.*, 2019), corresponding to the 1W hydration structure. From the peak shape information obtained via SAXS (Fig. 2), it was clear that the interlayer hydration state cannot be described by a single structure. The small spacing difference in the interlayer hydration structures (±0.3 nm) results in overlap of the characteristic peaks, making it difficult to accurately determine the various interlayer hydration structures of the GMZ powder via diffraction.

Small-angle scattering from upper and lower fractions of the dispersion (Fig. 3) indicated that the colloidal dispersion was not uniform. The scattering from the supernatant showed a broad indistinct peak, while the suspension of larger particles from the lower fraction of the dispersion exhibited prominent and characteristic peaks. The heavier solids collected from the colloid preparation procedure were dried at 40°C for 48 h and examined by SAXS (Fig. 4). The 1W hydration structure (*d*-space = 1.33 nm) was observed as the only characteristic peak of the precipitated GMZ. During the water absorption and swelling, the bentonite particles with a 1W hydration structure precipitated, while those with a tri-hydrated structure formed stable suspensions in the water. This difference may be caused by the interlayer defects in the bentonite as particles with severe defects do not swell fully and precipitate rapidly, even though swelling still occurs after water absorption. For the bentonite particles with a 0W structure, which have a low or no cation content (Brochard, 2021), their water absorption ability was weaker than that of the particles with 1W and 2W structures. Due to insufficient water absorption, these particles could not form stable suspensions in the water and precipitated.
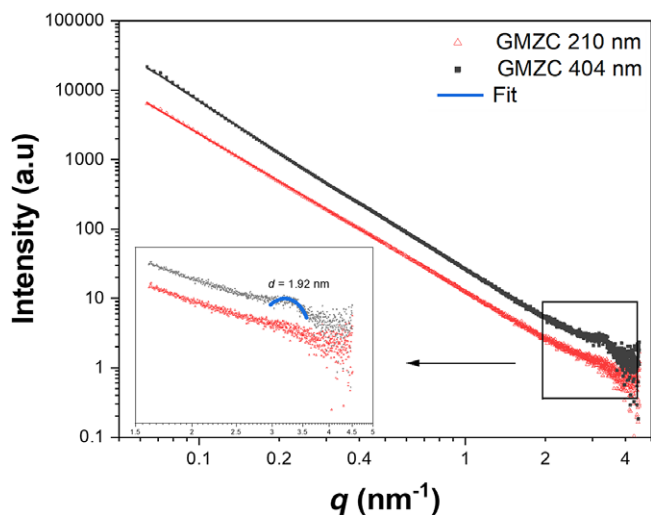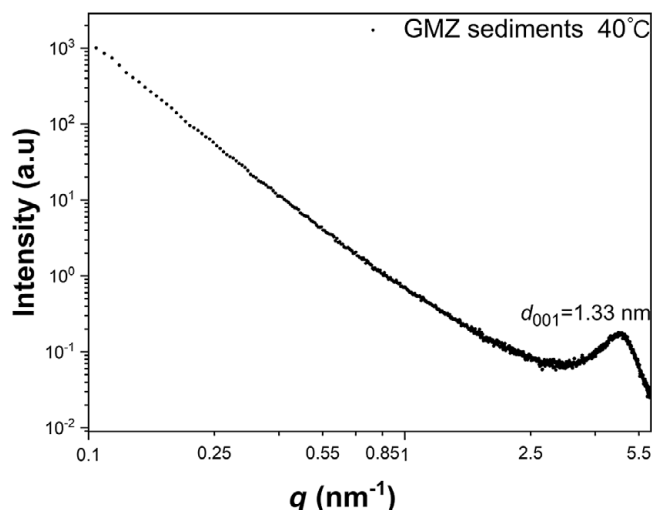

Figure 4. SAXS curves obtained from precipitates during the colloidal extraction process, dry at 40°C.

The stability of colloids at different pH values

To understand the effect of pH on the stability of the GMZC, the changes in the hydrodynamic diameter and zeta potential (ζ) of the colloids with pH were studied. In the acidic conditions (pH <5), the aggregation of the colloids was especially sensitive to salt concentration (Lagaly and Ziesmer, 2003). For this reason, no background electrolyte was added for these experiments. According to Fig. 5, the colloid size increased with decreasing pH, while ζ increased, indicating that the stability of the colloids decreased as the pH decreased. The faces and edges of the bentonite particles carry different charges: the face planar surfaces (silanol and aluminol sites) are at lower isoelectric points, while the edge surfaces (OH sites) are at higher isoelectric points (Svoboda, 2013). Active sites on both planar and edge surfaces are easily affected by ions:
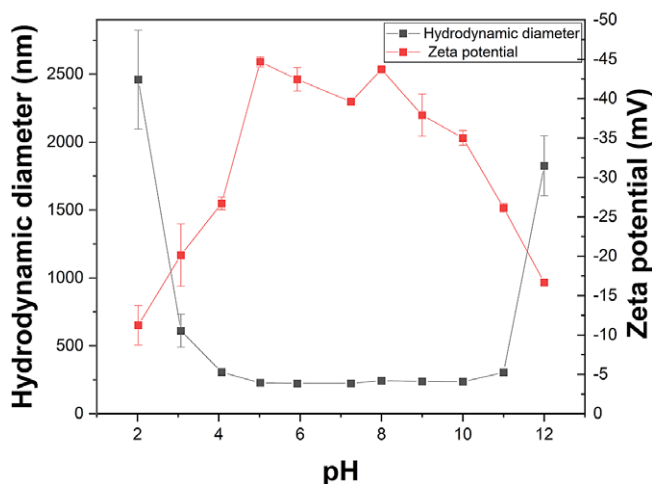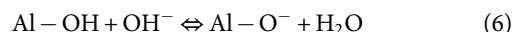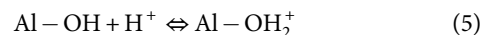
$$Al - OH + H^+ \Leftrightarrow Al - OH_2^+ \tag{5}$$

$$Al - OH + OH^- \Leftrightarrow Al - O^- + H_2O \tag{6}$$

Figure 3. SAXS curves obtained from upper (210 nm) and lower (404 nm) fractions of the colloidal dispersion.

Figure 5. The pH dependence of GMZC size and zeta potential without background electrolyte.

$$Si - OH + OH^- \Leftrightarrow Si - O^- + H_2O \qquad (7)$$

As the H^+ concentration was increased, the electrostatic effects became strong enough to trigger the attraction between the positively charged edges of the bentonite particles and the negatively charged faces, promoting the aggregation of colloidal particles and the transformation to a gel (Tombácz and Szekeres, 2004). At pH <3, the colloidal solution exhibited a high ionic strength without adding background electrolyte. This reduced the attraction between face–face compared with edge–face (Lagaly and Ziesmer, 2003); however, the hydrodynamic diameter of the colloids significantly increased. At this time, the aggregation of the colloidal particles occurred through edge–face stacking.

In alkaline conditions, repulsion between layers was expected, as the surfaces of all the colloidal particles were negatively charged. While $7 \leq pH \leq 11$ (Fig. 5), the hydrodynamic diameter of the colloidal particles did not change significantly. However, the hydrodynamic diameter of the colloidal particles increased at pH = 12, possibly due to the face-to-face aggregation of particles (Xian *et al.*, 2020).

Comparative analysis of the bentonite interlayer change with different cations

As the cation concentration increased, both hydrodynamic diameter and ζ of the particles gradually increased (Figs 6 and 7). For 10^{-4} mol L^{-1} Ca^{2+} and Mg^{2+} (the concentration refers to the concentration of groundwater in Beishan; Guo *et al.*, 2005), considerable aggregation of the colloidal particles occurred, along with significant stratification in the colloids.

With the introduction of higher-valence ions, the critical coagulation concentration of the colloidal precipitation decreased. With respect to Deryagin-Landau-Verwey-Overbeek (DLVO) theory, bivalent cations induced a greater reduction in the thickness of the colloidal double electric layer facilitating aggregation of the colloidal particles. Moreover, the hydration radius and ionic radius of the cations significantly affected the aggregation of the colloidal particles. When the difference between the ionic radius and the hydration radius was small, the
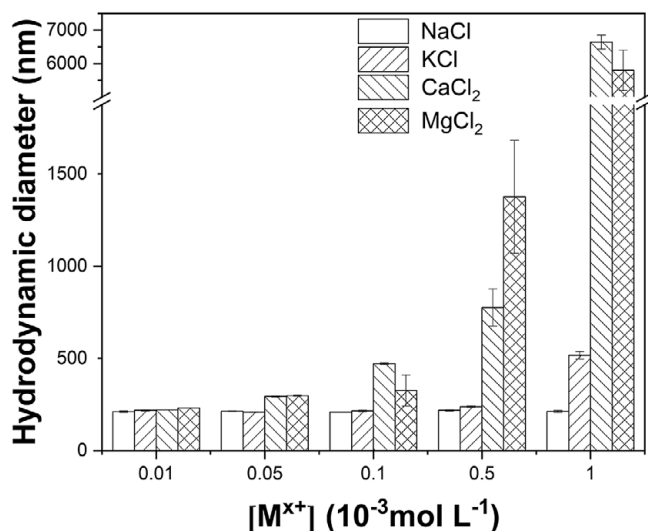
hydration shell was more easily detached as the ions bound to the colloidal particle surface, resulting in the formation of inner-sphere complexes between the ions and the particle surface (Xia *et al.*, 2017) and the ready aggregation of particles.

The powder XRD data (Fig. 8) showed that the main component of GMZ bentonite was montmorillonite, and the ions added during the experiment did not cause major structural change. For the sample with added Mg^{2+}, the diffraction peak was shifted (from $d_{001} = 1.5$ nm to $d_{001} = 1.54$ nm) and the intensity of the signal was reduced. The result of adding Ca^{2+} was to broaden the peak. Broadening of a diffraction peak could be due to a number of factors including layers of different basal space and small particle size. Furthermore, the effect shown here might also be explained by the disorder of the silicate sheets, the coexistence of large-span thick layers and the formation of a gel-like structure (Wilson *et al.*, 2004). Due to these complications, the colloidal dispersions were examined by the small-angle scattering technique, with an emphasis on observing the effect of ion exchange on the interlayer hydration structure (Fig. 9).

Figure 7. Effect of cations on the zeta potential of GMZC at pH = 8.5±0.05.

Figure 6. Effect of cations on the mean hydrodynamic diameter of GMZC at pH = 8.5 ±0.05.

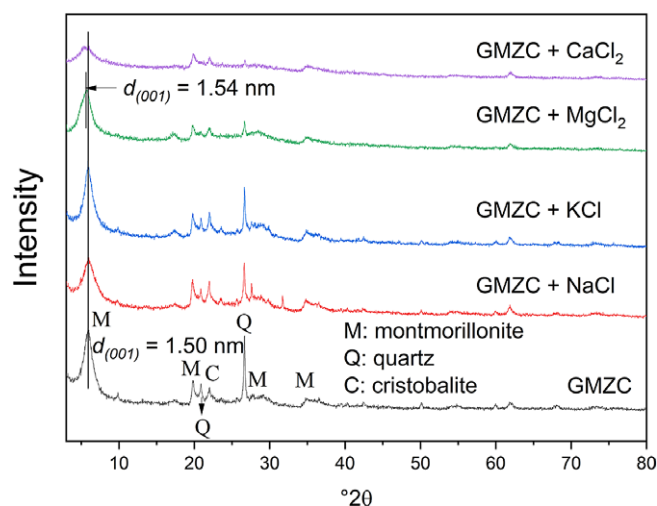**Figure 8.** Comparison of XRD patterns of GMZ colloidal powders with different ions ($c_{(M^{x+})} = 1 \times 10^{-4}$ mol L^{-1}).
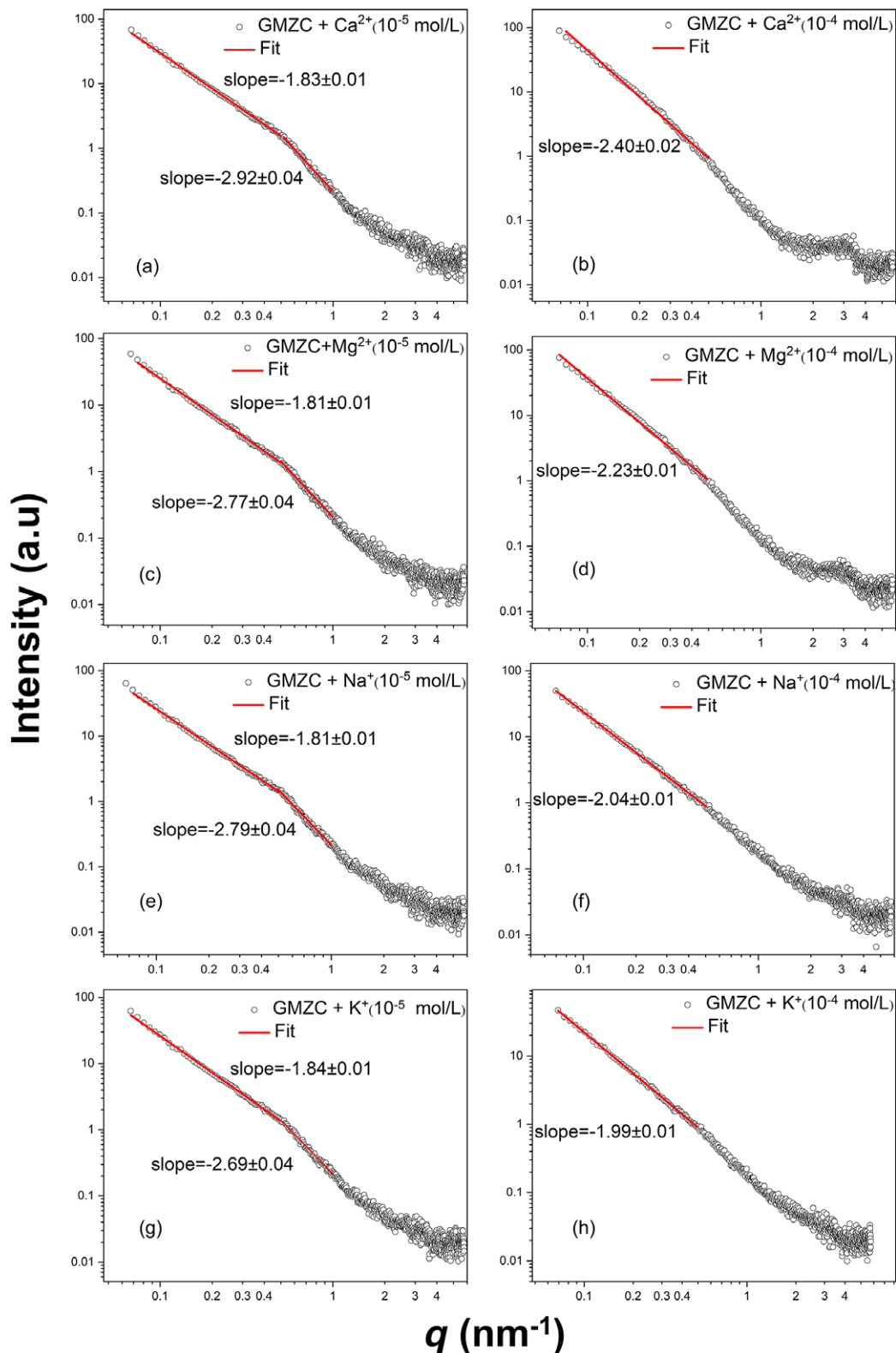
Figure 9. SAXS curves obtained from GMZC and chloride at different concentrations. The curves were fitted (lines) using a linear fitting model. The slope decreased, indicating aggregation of GMZ particles. (a) GMZC + Ca^{2+} 10^{-5} mol L^{-1}; (b) GMZC + Ca^{2+} 10^{-4} mol L^{-1}; (c) GMZC + Mg^{2+} 10^{-5} mol L^{-1}; (d) GMZC + Mg^{2+} 10^{-4} mol L^{-1}; (e) GMZC + K^{+} 10^{-5} mol L^{-1}; (f) GMZC + K^{+} 10^{-4} mol L^{-1}; (g) GMZC + Na^{+} 10^{-5} mol L^{-1}; (h) GMZC + Na^{+} 10^{-4} mol L^{-1}.

The introduction of Ca^{2+} or Mg^{2+} to the GMZC dispersion resulted in the following changes to the SAXS curve: (i) the power law slope between 0.06 nm^{-1} $\leq q \leq 0.5$ nm^{-1} decreased for low cation concentrations; (ii) the intensity of the diffraction peak lessened, and the peak shape became indistinct. As the concentration of Ca^{2+}/Mg^{2+} was raised, the power law slope decreased from $-1.83/-1.81$ to $-2.40/-2.23$, and the peak reappeared and became distinct.

These results suggest that at low concentrations, the interactions between the added divalent ions and the GMZC were dominated by ion exchange. That is, the Ca^{2+}/Mg^{2+} entered the interlayer spaces of the GMZC and disrupted the initially uniform hydration structure, resulting in a non-uniform interlayer spacing and weaker peak shape. The presence of these ions led to an enhanced scattering signal at around $q = 0.5$ nm^{-1} and reduced the power law index (e.g. Ca^{2+} from –1.83 to –2.96). Neither ζ nor the hydrodynamic diameter changed significantly at this time. As the concentration was further increased, the cations that entered the interlayer reached saturation. The interlayer spaces became uniform again and the peak shape reappeared. The cations remaining outside the interlayer spaces bonded to the surface of the GMZC particles via electrostatic interaction, rapidly reducing their surface ζ and the electrostatic repulsion between the particles. This disrupted the stability of the system, and the particles aggregated, as demonstrated by increased power law slope.

Similarly, the addition of potassium/sodium ions decreased the power law slope and weakened the peak shape. Unlike the behavior observed for Ca^{2+}/Mg^{2+}, as the concentration of K^+/Na^+ ions increased, the power law did not change significantly and the peak shape remained indistinct. For the monovalent ions Na^+ and K^+, at the same electrolyte concentration, the K^+-GMZC system showed a greater tendency to aggregate. Similar results were obtained by Wu-Quan *et al.* (2017) for Na^+/K^+ in soil suspensions. However, as demonstrated by the presence of divalent cations, ion exchange was the dominant mechanism at low concentrations.

For Na^+ and Ca^{2+} present in the alkaline condition (pH = 8.5), the electrostatic interaction among colloidal particles increased due to the presence of a surface charge. The relative dominance of Na^+ also led to an increase in the electrochemical bilayer thickness at the colloidal particle surface, thereby reducing the tendency of the particles to aggregate compared with dispersions that contained solely Ca^{2+} (Jiang *et al.*, 2012). The peaks reappeared after an excess of divalent cations was added (Fig. 9). For the mixed Na^+-Ca^{2+} case, the divalent cation may not have been dominant in terms of the concentration, but it still exerted a significant influence on the colloidal layered structure because the divalent cations were more strongly attracted to the interlayer spaces. When the cations became saturated in these spaces, they induced the formation of a regular layered structure more readily due to their attraction to the layers. Compared with divalent cations, monovalent cations displayed limited attraction to the colloidal layers in the concentration range of this experiment.

Conclusions

The effect of dispersion pH 2–12 and the addition of Na^+, K^+, Mg^{2+}, and Ca^{2+} (10^{-5} to 10^{-3} mol L^{-1}) on the lamellar structure and agglomerate morphology of GMZ bentonite colloids (~200 nm) were investigated by TEM, dynamic light scattering, zeta potential measurements, and small-angle X-ray scattering. At acidic pH, these colloids showed aggregation by edge-to-face attraction, while in the alkaline condition aggregation was achieved by face-to-face aggregation. The cation type and concentration played significant roles in the layered structure and morphology of aggregated GMZ colloids. Divalent cations at the highest concentration studied (10^{-3} mol L^{-1}), imparted order to the hydrated layered structure, even for dispersions that contained

mixed M^+-M^{2+} ions, emphasizing the influence of Ca^{2+} or Mg^{2+} on stabilizing bentonite barriers in HLW sites. The stability of GMZ bentonite colloids is one of the important pre-requisites for evaluating the influence of colloids on nuclide migration, and findings from this work would improve the understanding of stability of colloids at nanoscale levels. Therefore, the interlayer hydration structure and aggregation morphology of colloids obtained in this work can provide a valuable reference for safety assessment of HLW repository.

Author contributions. Zhaomin Tan: Conceptualization, Investigation, Formal analysis, Methodology, Writing - original draft. **Chengyun Fu:** Writing - review & editing, Validation. **Mark Julian Henderson:** Supervision, Writing - review & editing. **XuezhiDai:** Writing - review & editing. **Jianfeng Cheng:** Formal analysis, Validation. **Jingli Xie:** Investigation, Formal analysis. **Shan Zhu:** Supervision, Formal analysis, Writing - review & editing. **Minhao Yan:** Supervision, Resources, Conceptualization, Project administration.

References

Albarran, N., Degueldre, C., Missana, T., Alonso, U., García-Gutiérrez, M., & López, T. (2014). Size distribution analysis of colloid generated from compacted bentonite in low ionic strength aqueous solutions. *Applied Clay Science*, 95, 284–293. https://doi.org/10.1016/j.clay.2014.04.025

Baik, M.-H., Cho, W.-J., & Hahn, P.-S. (2007). Erosion of bentonite particles at the interface of a compacted bentonite and a fractured granite. *Engineering Geology*, 91, 229–239. https://doi.org/10.1016/j.enggeo.2007.02.002

Bouby, M., Geckeis, H., Lützenkirchen, J., Mihai, S., & Schäfer, T. (2011). Interaction of bentonite colloids with Cs, Eu, Th and U in presence of humic acid: a flow field-flow fractionation study. *Geochimica et Cosmochimica Acta*, 75, 3866–3880. https://doi.org/10.1016/j.gca.2011.04.015

Bradford, S. A., Simunek, J., Bettahar, M., van Genuchten, M. T., & Yates, S. R. (2003). Modeling colloid attachment, straining, and exclusion in saturated porous media. *Environmental Science & Technology*, 37, 2242–2250. https://doi.org/10.1021/es025899u

Brochard, L. (2021). Swelling of montmorillonite from molecular simulations: hydration diagram and confined water properties. *Journal of Physical Chemistry C*, 125, 15527–15543. https://doi.org/10.1021/acs.jpcc.1c02659

Bucher, F., & Müller-Vonmoos, M. (1989). Bentonite as a containment barrier for the disposal of highly radioactive wastes. *Applied Clay Science*, 4, 157–177. https://doi.org/10.1016/0169-1317(89)90006-9

Darda, S. A., Gabbar, H. A., Damideh, V., Aboughaly, M., & Hassen, I. (2021). A comprehensive review on radioactive waste cycle from generation to disposal. *Journal of Radioanalytical and Nuclear Chemistry*, 329, 15–31. https://doi.org/10.1007/s10967-021-07764-2

Degueldre, C., Pfeiffer, H.-R., Alexander, W., Wernli, B., & Bruetsch, R. (1996). Colloid properties in granitic groundwater systems. I: Sampling and characterisation. *Applied Geochemistry*, 11, 677–695.

Ferrage, E. (2016). Investigation of the interlayer organization of water and ions in smectite from the combined use of diffraction experiments and molecular simulations. a review of methodology, applications, and perspectives. *Clays and Clay Minerals*, 64, 348–373. https://doi.org/10.1346/ccmn.2016.0640401

Ferrage, E., Hubert, F., Baronnet, A., Grauby, O., Tertre, E., Delville, A., … & Levitz, P. (2018). Influence of crystal structure defects on the small-angle neutron scattering/diffraction patterns of clay-rich porous media. *Journal of Applied Crystallography*, *51*, 1311–1322. https://doi.org/10.1107/s160057671801052x

Ferrage, E., Kirk, C. A., Cressey, G., & Cuadros, J. (2007). Dehydration of Ca-montmorillonite at the crystal scale. Part 2. Mechanisms and kinetics. *American Mineralogist*, *92*, 1007–1017. https://doi.org/10.2138/am.2007.2397

Guinier, A., Fournet, G., Walker, C. B., & Yudowitch, K. L. (1979). *Small-Angle Scattering of X-rays*. New York: Wiley.

Guo, Y., Wang, J., Yu, S., Liu, S., & Zhong, Z. (2005). Chemical characteristics of groundwater and simulation of water-rock interaction in the preselection area of Maquan, Beishan, Gansu Province. *Earth Science Frontiers*, *S1*, 117–123.

Hong, W., Meng, J., Li, C., Yan, S., He, X., & Fu, G. (2020). Effects of temperature on structural properties of hydrated montmorillonite: experimental study and molecular dynamics simulation. *Advances in Civil Engineering*, *2020*, 8885215. https://doi.org/10.1155/2020/8885215

Huangfu, X., Jiang, J., Ma, J., Liu, Y., & Yang, J. (2013). Aggregation kinetics of manganese dioxide colloids in aqueous solution: influence of humic substances and biomacromolecules. *Environmental Science and Technology*, *47*, 10285–10292. https://doi.org/10.1021/es4003247

Huynh, K. A., & Chen, K. L. (2011). Aggregation kinetics of citrate and polyvinylpyrrolidone coated silver nanoparticles in monovalent and divalent electrolyte solutions. *Environmental Science and Technology*, *45*, 5564–5571. https://doi.org/10.1021/es200157h

Jiang, C.-L., Séquaris, J.-M., Vereecken, H., & Klumpp, E. (2012). Effects of inorganic and organic anions on the stability of illite and quartz soil colloids in Na-, Ca- and mixed Na–Ca systems. *Colloids and Surfaces A: Physicochemical and Engineering Aspects*, *415*, 134–141. https://doi.org/10.1016/j.colsurfa.2012.10.007

Kretzschmar, R., Holthoff, H., & Sticher, H. (1998). Influence of pH and humic acid on coagulation kinetics of kaolinite: a dynamic light scattering study. *Journal of Colloid and Interface Science*, *202*, 95–103.

Lagaly, G., & Ziesmer, S. (2003). Colloid chemistry of clay minerals: the coagulation of montmorillonite dispersions. *Advances in Colloid and Interface Science*, *100–102*, 105–128. https://doi.org/10.1016/s0001-8686(02)00064-7

Long, J. C. S., & Ewing, R. C. (2004). Yucca Mountain: earth-science issues at a geologic repository for high-level nuclear waste. *Annual Review of Earth and Planetary Sciences*, *32*, 363–401. https://doi.org/10.1146/annurev.earth.32.092203.122444

Meunier, A. (2006). Why are clay minerals small? *Clay Minerals*, *41*, 551–566. https://doi.org/10.1180/0009855064120205

Missana, T., Alonso, U., Albarran, N., García-Gutiérrez, M., & Cormenzana, J.-L. (2011). Analysis of colloids erosion from the bentonite barrier of a high level radioactive waste repository and implications in safety assessment. *Physics and Chemistry of the Earth*, *36*, 1607–1615. https://doi.org/10.1016/j.pce.2011.07.088

Missana, T., Alonso, U., Fernández, A. M., & García-Gutiérrez, M. (2018a). Analysis of the stability behaviour of colloids obtained from different smectite clays. *Applied Geochemistry*, *92*, 180–187. https://doi.org/10.1016/j.apgeochem.2018.03.010

Missana, T., Alonso, U., Fernández, A. M., & García-Gutiérrez, M. (2018b). Colloidal properties of different smectite clays: Significance for the bentonite barrier erosion and radionuclide transport in radioactive waste repositories. *Applied Geochemistry*, *97*, 157–166. https://doi.org/10.1016/j.apgeochem.2018.08.008

Missana, T., Alonso, U., & Turrero, M. J. (2003). Generation and stability of bentonite colloids at the bentonite/granite interface of a deep geological radioactive waste repository. *Journal of Contaminant Hydrology*, *61*, 17–31. https://doi.org/10.1016/S0169-7722(02)00110-9

Morida, K., Fukushi, K., Sakuma, H., & Tamura, K. (2023). Systematic comparison of the hydration and dehydration of Na^+-, K^+-, and NH_4^+-saturated montmorillonite, nontronite, hectorite, saponite, and Fe-saponite by in situ X-ray diffraction measurements. *Applied Clay Science*, *237*, 106898.

Pinnavaia, T., Rainey, V., Tzou, M.-S., & White, J. (1984). Characterisation of pillared clays by neutron scattering. *Journal of Molecular Catalysis*, *27*, 213–224.

Plaschke, M., Schäfer, T., Bundschuh, T., Ngo Manh, T., Knopp, R., Geckeis, H., & Kim, J. I. (2001). Size Characterization of bentonite colloids by different

methods. *Analytical Chemistry*, *73*, 4338–4347. https://doi.org/10.1021/ac010116t

Serie, I. N. E. (2022). Status and Trends in Spent Fuel and Radioactive Waste Management (no. NW-T-1.14, rev. 1). *IAEA Nuclear Energy Series*, 14.

SKB (2010). *Spent Nuclear Fuel for Disposal in the KBS-3 Repository*. Technical Report TR-10-13.

Svoboda, J. (2013). The experimental study of bentonite swelling into fissures. *Clay Minerals*, *48*, 383–389. https://doi.org/10.1180/claymin.2013.048.2.16

Swartzen-Allen, S. L., & Matijevic, E. (1976). Colloid and surface properties of clay suspensions. III. Stability of montmorillonite and kaolinite. *Journal of Colloid and Interface Science*, *56*, 159–167.

Tombácz, E., & Szekeres, M. (2004). Colloidal behavior of aqueous montmorillonite suspensions: the specific role of pH in the presence of indifferent electrolytes. *Applied Clay Science*, *27*, 75–94. https://doi.org/10.1016/j.clay.2004.01.001

Verma, P. K., Semenkova, A. S., Krupskaya, V. V., Zakusin, S. V., Mohapatra, P. K., Romanchuk, A. Y., & Kalmykov, S. N. (2019). Eu(III) sorption onto various montmorillonites: experiments and modeling. *Applied Clay Science*, *175*, 22–29. https://doi.org/10.1016/j.clay.2019.03.001

Villar, M. V., & Lloret, A. (2008). Influence of dry density and water content on the swelling of a compacted bentonite. *Applied Clay Science*, *39*, 38–49. https://doi.org/10.1016/j.clay.2007.04.007

Wang, J. (2010). High-level radioactive waste disposal in China: update 2010. *Journal of Rock Mechanics and Geotechnical Engineering*, *2*, 1–11. https://doi.org/10.3724/SP.J.1235.2010.00001

Wang, Y., Jiang, Q., Yang, Y., Cheng, J., Bao, C., Pan, Y., … & Tuo, X. (2022). Adsorption Properties of Cs(I) and Co(II) on GMZ bentonite colloids. *Nuclear Technology*, *208*, 1894–1907. https://doi.org/10.1080/00295450.2022.2083749

Wilson, J., Cuadros, J., & Cressey, G. (2004). An in situ time-resolved XRD-PSD investigation into Na-montmorillonite interlayer and particle rearrangement during dehydration. *Clays and Clay Minerals*, *52*, 180–191. https://doi.org/10.1346/ccmn.2004.0520204

Wu-Quan, D., Jia-Hong, H. E., Lei, W., Xin-Min, L. I. U., & Hang, L. I. (2017). Effect of nonclassical polarization of Na^+ and K^+ on the stability of soil colloidal particles in suspension. *Surface Review and Letters*, *24*. https://doi.org/10.1142/s0218625x18500191

Xia, T., Qi, Y., Liu, J., Qi, Z., Chen, W., & Wiesner, M. R. (2017). Cation-inhibited transport of graphene oxide nanomaterials in saturated porous media: the Hofmeister effects. *Environmental Science and Technology*, *51*, 828–837. https://doi.org/10.1021/acs.est.6b05007

Xian, D., Zhou, W., Pan, D., Du, L., Chang, M., Hu, N., … & Liu, C. (2020). Stability analysis of GMZ bentonite colloids: aggregation mechanism transition and the edge effect in strongly alkaline conditions. *Colloids and Surfaces A: Physicochemical and Engineering Aspects*, *601*. https://doi.org/10.1016/j.colsurfa.2020.125020

Xu, Z., Pan, D., Sun, Y., & Wu, W. (2018). Stability of GMZ bentonite colloids: aggregation kinetic and reversibility study. *Applied Clay Science*, *161*, 436–443. https://doi.org/10.1016/j.clay.2018.05.002

Yin, Z., Pan, D., Liu, P., Wu, H., Li, Z., & Wu, W. (2018). Sorption behavior of thorium(IV) onto activated bentonite. *Journal of Radioanalytical and Nuclear Chemistry*, *316*, 301–312. https://doi.org/10.1007/s10967-018-5716-5

Zhang, B. B., Miao, M. Y., Bai, J., Yuan, G. J., Jia, Y. Y., Han, Z. X., … & Su, H. Q. (2014). Researches on purification and sodium-modification of Ca-bentonite by tri-roller grinder. *Advanced Materials Research*, *962–965*, 809–813. https://doi.org/10.4028/www.scientific.net/AMR.962-965.809

Zhu, H., Fu, H., Yan, P., Li, X., Zhang, L., Wang, X., & Chai, C. (2022). Study on the release of GMZ bentonite colloids by static multiple light scattering technique. *Colloids and Surfaces A: Physicochemical and Engineering Aspects*, *640*. https://doi.org/10.1016/j.colsurfa.2022.128374

Zhu, S., Wang, Y., Zheng, C., Wang, Y., Tian, Q., Henderson, M. J., & Yan, M. (2022). Gaomiaozi bentonite colloids: Interactions with plutonium (IV) and zirconium (IV). *Colloids and Surfaces A: Physicochemical and Engineering Aspects*, *650*. https://doi.org/10.1016/j.colsurfa.2022.129636

Zuo, Q., Gao, X., Yang, J., Zhang, P., Chen, G., Li, Y., … & Wu, W. (2017). Investigation on the thermal activation of montmorillonite and its application for the removal of U(VI) in aqueous solution. *Journal of the Taiwan Institute of Chemical Engineers*, *80*, 754–760. https://doi.org/10.1016/j.jtice.2017.09.016